



LAWRENCE  
LIVERMORE  
NATIONAL  
LABORATORY

# Saturation of multi-beams laser-plasma interactions by stochastic ion heating

P. Michel, W. Rozmus, E. A. Williams, L. Divol, R.  
L. Berger, S. H. Glenzer, D. A. Callahan

December 13, 2012

Physics of Plasmas

## **Disclaimer**

---

This document was prepared as an account of work sponsored by an agency of the United States government. Neither the United States government nor Lawrence Livermore National Security, LLC, nor any of their employees makes any warranty, expressed or implied, or assumes any legal liability or responsibility for the accuracy, completeness, or usefulness of any information, apparatus, product, or process disclosed, or represents that its use would not infringe privately owned rights. Reference herein to any specific commercial product, process, or service by trade name, trademark, manufacturer, or otherwise does not necessarily constitute or imply its endorsement, recommendation, or favoring by the United States government or Lawrence Livermore National Security, LLC. The views and opinions of authors expressed herein do not necessarily state or reflect those of the United States government or Lawrence Livermore National Security, LLC, and shall not be used for advertising or product endorsement purposes.

# Saturation of multi-laser beams laser-plasma instabilities from stochastic ion heating

P. Michel,<sup>1</sup> W. Rozmus,<sup>2,1</sup> E.A. Williams,<sup>1</sup> L. Divol,<sup>1</sup> R.L. Berger,<sup>1</sup> S.H. Glenzer,<sup>1</sup> and D.A. Callahan<sup>1</sup>

<sup>1</sup>*Lawrence Livermore National Laboratory, Livermore, CA 94551*

<sup>2</sup>*Theoretical Physics Institute, University of Alberta, Edmonton, AB T6G2G7, Canada*

Cross-beam energy transfer (CBET) has been used as a tool on the National Ignition Facility (NIF) since the first energetics experiments in 2009 to control the energy deposition in ignition hohlraums and tune the implosion symmetry. As large amounts of power are transferred between laser beams at the entrance holes of NIF hohlraums, the presence of many overlapping beat waves can lead to stochastic ion heating in the regions where laser beams overlap [P. Michel et al., Phys. Rev. Lett. **109**, 195004 (2012)]. This increases the ion acoustic velocity and modifies the ion acoustic waves' dispersion relation, thus reducing the plasma response to the beat waves and the efficiency of CBET. This pushes the plasma oscillations driven by CBET in a regime where the phase velocities are much smaller than both the electron and ion thermal velocities. CBET gains are derived for this new regime and generalized to the case of multi ion species plasmas.

## I. INTRODUCTION

Overlapping multiple high power laser beams in plasmas can lead to cross-beam energy transfer (CBET), a process similar to Brillouin scattering in which the beat wave created by crossing laser beams drives a plasma oscillation that acts like a Bragg cell, scattering a beam in the direction of the other one [1, 2]. CBET has turned out to be a major player in inertial confinement fusion (ICF) experiments over the past few years, for both direct-drive and indirect-drive geometries. For indirect-drive experiments on the National Ignition Facility (NIF), control of CBET by wavelength separation tuning [3] has been demonstrated at the beginning of the National Ignition Campaign in 2009 [4, 5]. It has since then continuously been used as a tool to control the equatorial energy balance inside the ‘‘hohlraum’’ targets, and has even been developed further by adding additional wavelength tuning capabilities to control the polar symmetry or help mitigate backscatter by transferring laser energy away from the high-backscatter risk regions of the hohlraum and into the safer ones [6, 7]. On the other hand, for direct-drive experiments at the Omega facility, CBET moves energy from incoming laser beams into the refracted outer edges of outgoing laser beams, thus reducing the amount of laser energy being deposited into the coronal plasma [8, 9].

In CBET, the amount of power being transferred depends on the amplitude of the density modulation driven by the ponderomotive force of the beat wave, and on the proximity of the driven oscillation to an ion acoustic mode of the plasma. For two laser beams with frequencies  $\omega_m, \omega_n$  and wave vectors  $\mathbf{k}_m, \mathbf{k}_n$  driving a beat wave with wave vector  $\mathbf{k} = \mathbf{k}_m - \mathbf{k}_n$  and frequency  $\omega_k = \omega_m - \omega_n$ , the coupling is thus maximum when the phase velocity of the beat wave in the frame of the plasma,  $v_k = (\omega_k - \mathbf{k} \cdot \mathbf{V})/k$  (where  $\mathbf{V}$  is the plasma flow), is equal to the plasma sound speed  $c_s$ , which will drive a plasma oscillation  $\delta n_e/n_e$  (where  $n_e$  is the electron density) matching the ion acoustic wave dispersion relation (cf. Fig. 1). This is equivalent to a Bragg cell, with

a modulation of the refractive index  $N = \sqrt{1 - n_e/n_c}$  (where  $n_c$  is the critical density for the laser wavelength) traveling at the sound speed of the medium. On NIF, CBET is controlled by using different wavelengths for different cones of laser beams, i.e.  $v_k$  is adjusted via  $\omega_k$ ; typically, the corresponding wavelength shift  $\Delta\lambda_k$  (with  $\omega_k/\omega_0 = \Delta\lambda_k/\lambda_0$ , where  $\omega_0$  and  $\lambda_0$  are the laser frequency and wavelength) is a few Å, with  $v_k < c_s$ . Whereas on Omega, where all the beams have identical wavelength ( $\omega_k=0$ ), CBET occurs because beams cross at the Mach 1 surface of the expanding coronal plasma where  $\mathbf{k} \cdot \mathbf{V} = kc_s$  (i.e.  $v_k = c_s$  in the plasma frame).

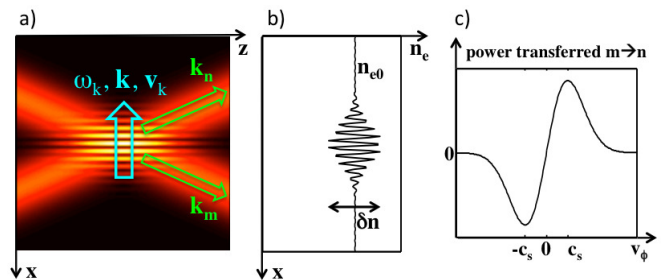


FIG. 1. Basic mechanism for CBET: a) two crossing laser beams with frequencies  $\omega_m, \omega_n$  and wave vectors  $\mathbf{k}_m, \mathbf{k}_n$  drive a beat wave with frequency  $\omega_k = \omega_m - \omega_n$ , wave vector  $\mathbf{k} = \mathbf{k}_m - \mathbf{k}_n$ , and phase velocity  $v_k = (\omega_k - \mathbf{k} \cdot \mathbf{V})/k$  in the frame of the plasma ( $\mathbf{V}$  is the plasma flow velocity); b) the ponderomotive force from the beat wave drives a density modulation in the plasma, and hence a refractive index modulation, traveling at  $v_k$ ; c) if  $|v_k| = c_s$ , the refractive index modulation acts as a Bragg cell scattering one laser beam in the direction of the other (i.e. energy transfer); being able to control  $v_k$ , e.g. via the frequency shift  $\omega_k$  between the beams, allows to set the direction of power transfer (via the sign) and its amplitude (via the proximity of  $v_k$  to  $c_s$ ).

CBET on NIF was initially predicted to be observable and controllable because of the small amplitudes of the density modulations created by the beat waves, preventing non-linear effects from occurring but still being large enough to allow significant amounts of transfer due to

cumulative effects from multiple crossing, taking place in fairly uniform plasmas over very long ( $\sim$  mm) distances [3, 5, 10, 11]. The ion acoustic waves are typically strongly damped, leading to broad resonance regions (as schematically represented in Fig. 1c) and amplification gains being less sensitive to gradients or non-uniformities in the plasma.

Calculations using the linear response of an ion wave to the beat ponderomotive force were in decent agreement with the 2009 experiments where NIF was typically delivering 200 TW of peak laser power with small wavelength separations ( $\Delta\lambda=1.5 - 5 \text{ \AA}$ ) leading to small amounts of transfer. However, in more recent experiments, where peak laser power is usually between 400 and 500 TW and where large amounts of power transfer are required to achieve symmetric implosions of the DT fuel capsule ( $\Delta\lambda=6$  to  $9 \text{ \AA}$ ), linear calculations fail to reproduce the experimental observables, and in fact usually predict a full pump depletion of the NIF “outer beams” which has never been seen in experiments. An artificial limiter on the amplitude of the density modulations  $\delta n/n$  driven by the beat waves has thus been introduced in the design calculations in order to recover some level of predictive capability [6, 8, 12]; it is however purely empirical and lacking physics justification, and the values at which one needs to saturate the waves are too low to be physically justified ( $\delta n/n \simeq 10^{-4}$ ).

It was recently discovered that even though the density modulations driven by CBET are small, having many of these modulations coexisting in the same plasma can lead to weak turbulence effects, which together with ion-ion collisions can lead to turbulent ion heating in the region where the laser beams overlap [13]. The resulting changes in hydrodynamics condition can in turn saturate CBET by modifying the ion acoustic dispersion relation.

In this article, we expand our analysis of CBET saturation from stochastic ion heating, exploring the new regime of driven plasma oscillations far from resonance and generalizing to multi-ion species plasmas. The following section provides detailed analysis of the oscillations driven by CBET for typical NIF conditions, and the associated CBET linear gains. Sec. III presents a new “quasi-linear” particle code and shows results on ion heating for multi-ion species plasmas. Finally, Sec. IV shows the dependence of CBET gains to wavelength shifts for NIF conditions, and gives new expressions for linear gains in the small  $\Delta\lambda$  limit, i.e. when the ions have been sufficiently heated so that the beat waves’ phase velocities become smaller than the ion phase velocity. Localization of heating rates and flow acceleration in NIF hohlraums are also presented. In the appendix we show the derivation of a reduced fluid model from quasi-linear theory and calculate the expression of electron heating; it is shown that electron heating from weak turbulence should be negligible for typical NIF conditions, the energy deposited in the plasma from wave-particle interaction going primarily in the ions.

## II. LINEAR EXPRESSIONS FOR THE DRIVEN PLASMA OSCILLATIONS AND CONVECTIVE GAINS FOR NIF CONDITIONS

In this section we derive the expressions of the plasma oscillations driven by beat waves between crossing pairs of laser beams, as well as the convective gains for laser scattering off these oscillations, and give typical values for NIF conditions.

### A. Density perturbation

Each pair of crossing laser beams ( $m, n$ ) drives a beat wave with wave vector  $\mathbf{k} = \mathbf{k}_m - \mathbf{k}_n$  and frequency  $\omega_k = \omega_m - \omega_n$ . If the two beams have different frequencies, then  $\omega_k \neq 0$  and the beat wave has a phase velocity  $\mathbf{v}_k = \mathbf{k}\omega_k/k^2$ . In the rest of the paper, we will assume that the frequency shift between the laser beams is small,  $\omega \ll \omega_m, \omega_n$ , so that  $k \simeq 2k_0 \sin(\theta_k/2)$ , where  $k_n \simeq k_m = k_0$  is the lasers’ wave numbers, and  $\theta_k$  is the angle between the two laser beams.

The ponderomotive potential from the beat wave  $\varphi_p$  acts on the electrons of the plasma, creating a charge separation and thus an electrostatic potential  $\phi$  exerted on both the electrons and the ions. The forces exerted on the electrons and the ions are thus respectively:  $\mathbf{F}_e = e\nabla(\varphi_p + \phi)$  and  $\mathbf{F}_i = -q_i\nabla\phi$ , where  $q_i = Ze$  is the charge of the ion.

Poisson’s equation connects the electrostatic potential  $\phi$  to the resulting density perturbation in the plasma:  $-\nabla^2\phi = 4\pi\sum_{\alpha}q_{\alpha}\delta n_{\alpha}$ , where the summation is taken over the species (i.e.  $\alpha = e$  or  $i$ ). In the following we will assume that the potentials have an envelope slowly varying in space and time compared to the rapid oscillation of the beat wave:  $\varphi_p = \frac{1}{2}\hat{\varphi}_p \exp[i\psi] + c.c.$ ,  $\phi = \frac{1}{2}\hat{\phi} \exp[i\psi_k] + c.c.$ , where  $\psi_k(\mathbf{r}, t) = \mathbf{k} \cdot \mathbf{r} - \omega_k t$  is the phase of the beat wave (in the rest of the paper, the “hat” notation will refer to a complex enveloped quantity, i.e.  $f = |\hat{f}| \cos(\psi)$  where the envelope  $\hat{f}$  is slowly varying compared to the phase  $\psi$ ). The expression for the density perturbation can then be obtained from the Vlasov equation:

$$\frac{\partial f_{\alpha}}{\partial t} + \mathbf{v} \cdot \nabla f_{\alpha} + \frac{\mathbf{F}_{\alpha}}{m_{\alpha}} \cdot \frac{\partial f_{\alpha}}{\partial \mathbf{v}} = 0, \quad (1)$$

where  $\alpha = e$  or  $i$ . Separating the response to the beat wave’s potential from the rest of the distribution, i.e.  $f_{\alpha}(\mathbf{r}, \mathbf{v}, t) = f_{\alpha 0}(\mathbf{r}) + \delta f_{\alpha}(\mathbf{r}, \mathbf{v}, t)$ , with  $\delta n_{\alpha}(\mathbf{r}, t) = \int d^3v \delta f_{\alpha}(\mathbf{r}, \mathbf{v}, t)$  and with the density perturbation being enveloped similarly to the potential that is driving it, i.e.  $\delta n_{\alpha} = \frac{1}{2}\delta\hat{n}_{\alpha} \exp[i\psi_k] + c.c.$  and  $f_{\alpha} = \frac{1}{2}\hat{f}_{\alpha} \exp[i\psi_k] + c.c.$ , gives:

$$\delta\hat{n}_{\alpha} = -\frac{q_{\alpha}}{m_{\alpha}}(\phi + \delta_{\alpha e}\varphi_p) \int \mathbf{k} \cdot \frac{\partial f_{\alpha 0}}{\partial \mathbf{v}} \frac{d^3v}{\omega_k - \mathbf{k} \cdot \mathbf{v}}, \quad (2)$$

where  $\alpha = e$  or  $i$  and  $\delta_{\alpha e}$  is a Kronecker delta (i.e. the ponderomotive potential is only acting on the electrons).

Using the usual definitions for the electron and ion susceptibilities,

$$\chi_{ek} = \frac{4\pi q_e^2}{k^2 m_e} \int \mathbf{k} \cdot \frac{\partial f_e}{\partial \mathbf{v}} \frac{d^3 v}{\omega_k - \mathbf{k} \cdot \mathbf{v}}, \quad (3)$$

$$\chi_{ik} = \sum_j \frac{4\pi q_j^2}{k^2 m_j} \int \mathbf{k} \cdot \frac{\partial f_i}{\partial \mathbf{v}} \frac{d^3 v}{\omega_k - \mathbf{k} \cdot \mathbf{v}}, \quad (4)$$

where the summation for the ion susceptibility is over the different ion species  $j$ , and using Poisson's equation gives:

$$\phi(1 + \chi_{ek} + \chi_{ik}) = -\varphi_p \chi_{ek}. \quad (5)$$

The electron density perturbation can then be expressed as:

$$\frac{\delta \hat{n}_e}{n_e} = -\hat{\varphi}_p K_k \frac{k^2 c^2}{\omega_{pe}^2}, \quad (6)$$

where  $K_k = \chi_{ek}(1 + \chi_{ik})/(1 + \chi_{ek} + \chi_{ik})$  and  $\omega_{pe}$  is the background electron plasma frequency.

The ponderomotive potential can be expressed for arbitrary polarizations of the two crossing laser beams  $m$ ,  $n$ . Let  $(\mathbf{x}_m, \mathbf{y}_m, \mathbf{z}_m)$  and  $(\mathbf{x}_n, \mathbf{y}_n, \mathbf{z}_n)$  be the two beams' bases, where  $\mathbf{z}$  is the propagation direction of the beam. The normalized vector potentials for the two beams can be decomposed onto the two transverse directions  $\mathbf{x}$  and  $\mathbf{y}$ :

$$\mathbf{a}_m = \frac{1}{2} [\hat{a}_{mx} \mathbf{x}_m + \hat{a}_{my} \mathbf{y}_m] e^{i\psi_m} + c.c., \quad (7)$$

$$\mathbf{a}_n = \frac{1}{2} [\hat{a}_{nx} \mathbf{x}_n + \hat{a}_{ny} \mathbf{y}_n] e^{i\psi_n} + c.c., \quad (8)$$

where  $\psi_m = \mathbf{k}_m \cdot \mathbf{r} - \omega_m t$  is the phase of the beam  $m$  and  $\psi_n$  is the phase of beam  $n$ . The vector potentials are normalized in the usual way, as  $a = v_{osc}/c$  where  $v_{osc}$  is the electron quiver velocity in the laser field, i.e.  $a = (e/mc\omega)E$  where  $\omega$  and  $E$  are the laser's frequency and electric field; this is also equivalent to  $|\hat{a}| = 0.855 \times 10^{-9} \lambda_\mu \sqrt{I}$  where  $I$  is the laser intensity in  $\text{W}/\text{cm}^2$  and  $\lambda_\mu$  its wavelength in microns.

The ponderomotive potential for the total electric field is:

$$\phi_p = -\frac{1}{2} \frac{e}{r_e} (\mathbf{a}_m + \mathbf{a}_n)^2, \quad (9)$$

where  $r_e = e^2/m_e c^2$  is the classical electron radius.

Taking only the beat component  $\varphi_p = \frac{1}{2} \hat{\varphi}_p \exp[i\psi_k] + c.c.$  oscillating at  $\psi_k = \psi_m - \psi_n$  gives:

$$\hat{\varphi}_p = -\frac{1}{2} \frac{e}{r_e} \left[ \hat{a}_{mx} \hat{a}_{nx}^* \mathbf{x}_m \cdot \mathbf{x}_n + \hat{a}_{mx} \hat{a}_{ny}^* \mathbf{x}_m \cdot \mathbf{y}_n + \hat{a}_{my} \hat{a}_{nx}^* \mathbf{y}_m \cdot \mathbf{x}_n + \hat{a}_{my} \hat{a}_{ny}^* \mathbf{y}_m \cdot \mathbf{y}_n \right]. \quad (10)$$

Let us first consider the case where the two beams are linearly polarized, for example along their  $\mathbf{x}$  axes:  $\mathbf{a}_m = \frac{1}{2} \hat{a}_m \mathbf{x} \exp[i\psi_m] + c.c..$  In this case, we simply have:

$$|\hat{\varphi}_p|_{\parallel} = \frac{1}{2} \frac{e}{r_e} |\hat{a}_m| |\hat{a}_n| \cos \theta_{mn} \quad (11)$$

where  $\theta_{mn} = \mathbf{x}_m \cdot \mathbf{x}_n$  is the angle between the two polarization vectors of the beams.

On the other hand, most large scale facilities have polarization mixing schemes. On NIF, laser beams are grouped into quadruplets or "quads", as shown in Fig. 2. Two of the beams in a quad have their polarization direction (say,  $\mathbf{y}_m$ ) along the radial direction  $\theta$ , and the other two beams are polarized perpendicularly with  $\mathbf{x}_m$  along the azimuthal direction  $\phi$  (cf. Fig. 2).

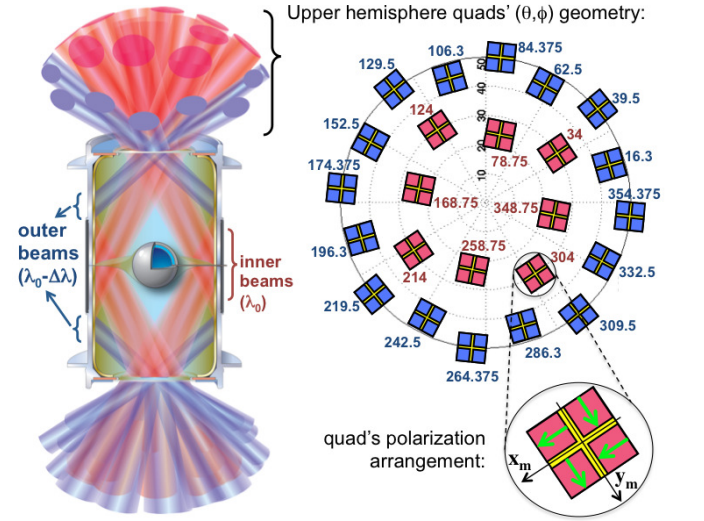


FIG. 2. NIF geometry: 192 laser beams grouped in 48 quadruplets or "quads" enter the cylindrical "hohlraum" cavity through the laser entrance holes (LEH) at both ends of the hohlraum. The "inner beams", at  $23.5^\circ$  and  $30^\circ$  from the hohlraum axis and hitting the hohlraum wall near the waist, are shown in red, whereas the "outer beams", at  $44.5^\circ$  and  $50^\circ$  from axis, are shown in blue and hit near the LEH. Also shown is a polar view of the 24 quads from the upper hemisphere; the number next to each quad is its azimuthal angle in degree. The zoomed-in view of one of the quads shows the "checkerboard" polarization arrangement of the 4 beams in a quad.

The fields between the four beams are spatially smoothed by phase plates and are uncorrelated from one-another, so taking an ensemble average on Eq. (10) (i.e. averaging in the transverse spatial dimensions over multiple speckles widths) gives:

$$|\hat{\varphi}_p|_{P.S.}^2 = \frac{e^2}{4r_e^2} \left[ |\hat{a}_{mx}|^2 |\hat{a}_{nx}|^2 (\mathbf{x}_m \cdot \mathbf{x}_n)^2 + |\hat{a}_{mx}|^2 |\hat{a}_{ny}|^2 (\mathbf{x}_m \cdot \mathbf{y}_n)^2 + |\hat{a}_{my}|^2 |\hat{a}_{nx}|^2 (\mathbf{y}_m \cdot \mathbf{x}_n)^2 + |\hat{a}_{my}|^2 |\hat{a}_{ny}|^2 (\mathbf{y}_m \cdot \mathbf{y}_n)^2 \right], \quad (12)$$

where the cross-terms ensemble-average to zero (“P.S.” in the subscript refers to polarization smoothing).

Assuming that the total power is equally distributed between the four beams in a quad, i.e.  $|\hat{a}_{mx}|^2 = |\hat{a}_{my}|^2 = \frac{1}{2}|\hat{a}_m|^2$ , gives:

$$|\hat{\varphi}_p|_{P.S.}^2 = \frac{e^2}{16r_e^2} |\hat{a}_m|^2 |\hat{a}_n|^2 \left[ (\mathbf{x}_m \cdot \mathbf{x}_n)^2 + (\mathbf{x}_m \cdot \mathbf{y}_n)^2 + (\mathbf{y}_m \cdot \mathbf{x}_n)^2 + (\mathbf{y}_m \cdot \mathbf{y}_n)^2 \right]. \quad (13)$$

Noticing that  $(\mathbf{x}_m \cdot \mathbf{x}_n)^2 + (\mathbf{x}_m \cdot \mathbf{y}_n)^2 = 1 - (\mathbf{x}_m \cdot \mathbf{z}_n)^2$ , etc., finally gives:

$$|\hat{\varphi}_p|_{P.S.}^2 = \frac{e^2}{16r_e^2} |\hat{a}_m|^2 |\hat{a}_n|^2 [1 + \cos^2(\theta_k)], \quad (14)$$

where  $\theta_k = \mathbf{z}_m \cdot \mathbf{z}_n$  is the angle between the quads  $m$  and  $n$ .

In summary, the plasma oscillation driven by each beat wave between two NIF quads can be expressed as:

$$\left| \frac{\delta \hat{n}_e}{n_e} \right| = |K_k| \sin^2 \left( \frac{\theta_k}{2} \right) \frac{1 - \tilde{n}_0}{\tilde{n}_0} |\hat{a}_m| |\hat{a}_n| \sqrt{1 + \cos^2 \theta_k} \quad (15)$$

where  $\tilde{n}_0 = n_0/n_c$  is the background electron density normalized to the critical density for the laser frequency, and  $\theta_k$  is the angle between the two quads’  $k$ -vectors.

It can easily be shown that for two laser beams with random polarizations in the  $(\mathbf{x}, \mathbf{y})$  plane, the same expression as for two NIF quads is obtained.

The amplitude of the corresponding electrostatic potential is:

$$|\hat{\phi}_k| = \frac{e}{4r_e} \left| \frac{\chi_{ek}}{1 + \chi_{ek} + \chi_{ik}} \right| |\hat{a}_m| |\hat{a}_n| \sqrt{1 + \cos^2 \theta_k}. \quad (16)$$

The formula for NIF quads, averaging the speckles and polarization effects, is appropriate as long as: i) the laser spots from the four beams are well superimposed in the plasma (far-field), so that all polarizations are present at any point in the far field; ii) the waves remain small, so that non-linear correlations between initially uncorrelated fields can be neglected; and iii) the plasma conditions remain nearly constant over a few speckle widths (i.e. a few tens of microns for NIF’s F/8 aperture and 351 nm wavelength).

## B. Linear gains for NIF parameters

The linear convective CBET gains between two laser beams  $(m, n)$  can be derived from the wave equation for the total vector potential  $\mathbf{a} = \mathbf{a}_m + \mathbf{a}_n$ :

$$(\partial_t^2 + \omega_{p0}^2 - c^2 \nabla^2) \mathbf{a} = -\omega_{p0}^2 \frac{\delta n}{n_0} \mathbf{a}, \quad (17)$$

where  $\omega_{p0}^2 = 4\pi e^2 n_0 / m_e$  is the background electron plasma frequency with  $n_0$  the background electron density such that  $n_e = n_0 + \delta n$ . Collecting the terms in phase with  $\psi_m$  and aligned with  $\mathbf{x}_m$  (i.e. proportional to  $\exp[i\psi_m] \mathbf{x}_m$ ) and applying the usual paraxial and steady state approximations gives:

$$\left( \partial_z + \frac{k'_m}{2k_m} \right) \hat{a}_{mx} = -i \frac{\omega_{p0}^2}{4k_m c^2} \frac{\delta \hat{n}}{n_0} (\hat{a}_{nx} \mathbf{x}_m \cdot \mathbf{x}_n + \hat{a}_{ny} \mathbf{x}_m \cdot \mathbf{y}_n) \quad (18)$$

where  $k'_m = \partial_z k_m$  is the  $z$ -derivative of the wavenumber of the beam  $m$  (when a density gradient is present).

Using the expression of  $\delta \hat{n}$  from Eqs. (6) with the full expression for the ponderomotive potential from Eq. (10), and averaging the speckles and crossed polarizations effects as was done for the expression of the density perturbation gives the following formula for two NIF quads:

$$\partial_z |\hat{a}_m|^2 = -\text{Im}(K_k) \frac{k^2}{8k_m} |\hat{a}_m|^2 |\hat{a}_n|^2 (1 + \cos^2 \theta_k). \quad (19)$$

Assuming small gains from multiple quads, as is typical on NIF, one can generalize the formula for the convective gain of a quad  $m$  from all the other quads  $n$  it encounters along its way:

$$\partial_z |\hat{a}_m|^2 = |\hat{a}_m|^2 \sum_n \gamma_{mn}, \quad (20)$$

The total gain rate for the quad  $m$  is the sum of the contributions from the intersecting quads,  $\Gamma_m = \sum_n \gamma_{mn}$ , with:

$$\gamma_{mn} = -\text{Im}(K_k) \frac{k^2}{8k_m} |\hat{a}_n|^2 (1 + \cos^2 \theta_k). \quad (21)$$

## C. Typical parameters for NIF conditions

As shown in Fig. 2, 24 quads overlap at each laser entrance hole (LEH) as they enter a NIF hohlraum. Eight are “inner” quads (shown in red), hitting near the hohlraum waist: 4 inner quads propagate at  $23.5^\circ$  from axis and 4 propagate at  $30^\circ$ . The other 16 quads are “outer” quads (shown in blue), with 8 of them propagating at  $44.5^\circ$  and the other 8 at  $50^\circ$  from axis.

Fig. 3 shows the amplitudes of the density modulations and the gain rates for typical NIF conditions at the LEH during the beginning of the main laser pulse. The “inner” and “outer” quads have intensities of  $5 \times 10^{14}$  and  $10^{15}$  W/cm<sup>2</sup> respectively. We assume a wavelength separation between inner and outer beams of  $\Delta\lambda = 6\text{\AA}$ . This is typical of current NIF experiments, as required to transfer enough energy from the outer beams to the inner beams in order to achieve symmetric implosions.

We use typical LEH plasma conditions at the beginning of the main pulse: the background electron density is  $n_0 = 3\% n_c$  and the electron and ion temperatures are 2.8

and 0.8 keV respectively. The plasma is composed of fully ionized helium ( $Z=2$ ). We also assume that the electrons and ions are Maxwellian, so the susceptibilities can be expressed using the derivative of the plasma dispersion function  $Z'$ :

$$\chi_{ek} = -\frac{1}{2(k\lambda_{De})^2} Z' \left[ \frac{\omega_k - \mathbf{k} \cdot \mathbf{V}}{\sqrt{2}kv_{Te}} \right], \quad (22)$$

$$\chi_{ik} = \sum_j -\frac{\alpha_j}{2(k\lambda_{De})^2} Z' \left[ \frac{\omega_k - \mathbf{k} \cdot \mathbf{V}}{\sqrt{2}kv_{Tij}} \right], \quad (23)$$

where  $\mathbf{V} = \langle \mathbf{v} \rangle$  is the average (flow) velocity, and  $\alpha_j = Z_j^* T_e / T_{ij}$  with  $Z_j^* = f_j Z_j^2 / \bar{Z}$  and  $f_j$ ,  $Z_j$ ,  $T_{ij}$  are the fraction, atomic number and temperature of the ion specie  $j$ . The average charge is  $\bar{Z} = \sum_j f_j Z_j$ , so that  $n_e = \bar{Z} n_i$ .

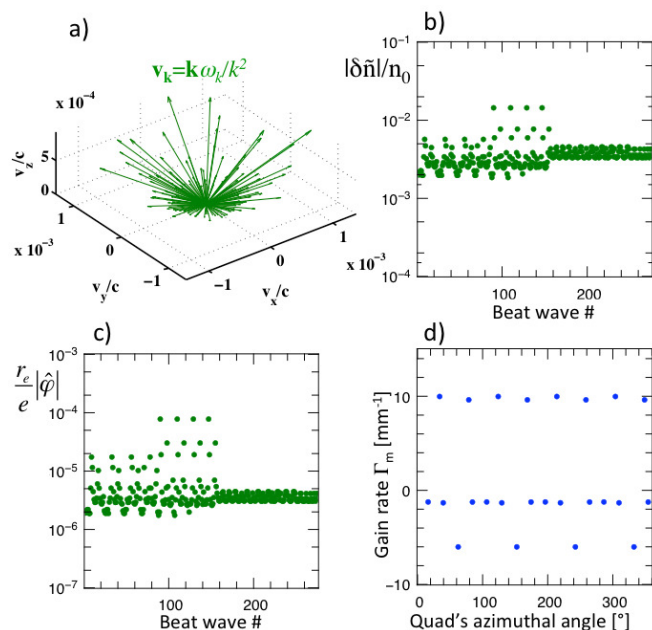


FIG. 3. a) phase velocities of the 276 beat waves created by crossing pairs of quads, from the 24 quads overlapping at each LEH of a NIF hohlraum ( $z$  is the hohlraum axis; 148 of the beat waves actually have no phase velocity since they are created by quads with similar wavelengths); b) amplitudes of the density fluctuations created by the beat waves; c) electrostatic potentials driven by the beat waves (normalized to  $e/r_e$ ); d) gain rates  $\Gamma_m$  for each of the 24 quads (such that  $\partial_z |\hat{a}_m|^2 = \Gamma_m |\hat{a}_m|^2$ ), ordered against the azimuthal angle of the quads in the NIF chamber (cf. Fig. 2).

The presence of 24 quads overlapping in the same  $\sim \text{mm}^3$  volume at the LEH leads to 276 possible pairs between quads and therefore 276 driven beat waves. The 276 beat waves' phase velocities are shown in Fig. 3a. In our example, we assumed two different wavelengths between cones of laser beams, as shown in Fig. 2 (NIF

can also operate with three different wavelengths, to tune higher-order asymmetry modes [6, 7, 14]). Therefore, out of the 276 possible pairs, 128 are composed of an inner and an outer quad and thus have a finite phase velocity (since the quads have different wavelengths, i.e.  $\omega_k \neq 0$ ), and the 148 others are between two inner or two outer and thus have zero phase velocity. As can be seen in Fig. 3a, the phase velocities range from 0 to  $\sim c/1000$  and exhibit axis-symmetry around  $z$ , the hohlraum axis. The velocity vectors are all oriented towards the exterior of the hohlraum (i.e. they all have a positive  $v_z$  component).

Fig. 3b shows the density perturbations from these 276 beat waves, which are typically of the order of  $|\delta \hat{n}|/n_0 \approx 10^{-3}$ . The electrostatic potentials driven by these waves are shown in Fig. 3c, and typically range from  $10^{-6}$  up to almost  $10^{-4} \times e/r_e$ . Finally, the exponential gain rates  $\Gamma_m$  for each of the 24 quads are shown in Fig. 3d, as a function of the azimuthal angle of the quad (as represented on the polar map from Fig. 2). The 8 inner quads have positive gain rates of about  $10 \text{ mm}^{-1}$ , whereas the 16 outer beams have negative values (because they give energy to the inner beams).

Note that the gain rates as calculated from such linear calculations are very high: for uniform plasma conditions and an interaction region being 0.5 to 1 mm long between all 24 quads, these gains would lead to full depletion of the outer beams (i.e. the inner beams would have their power increase by  $\times 3$ ). This has never been observed in the experiments, where various measurement methods from different diagnostics systematically give estimates of a 50% to 100% power increase on the inner beams (i.e. 25% to 50% power reduction on the outer beams) as required for symmetric implosions.

### III. QUASI-LINEAR PARTICLE CODE

In order to investigate how kinetic effects and weak turbulence can influence the CBET gains for NIF conditions, we have developed a particle code specifically adapted to our situation, where particles interact with a very large number of small amplitude externally-driven waves. The code tracks particles evolving in multiple overlapping electrostatic fields created by the ponderomotive potentials of the 276 beat waves resulting from all the couplings between pairs of quads, among 24 quads. The electrostatic fields evolution is done in the spirit of quasi-linear theory, by taking the spatial average of the distribution function of particles.

The interaction of particles with each driven wave therefore includes nonlinear effects from particle trapping, which is generally the most efficient saturation mechanism for ion acoustic waves [11]. On the other hand, the effects from many overlapping electrostatic waves is treated in a quasi-linear fashion, i.e. it accounts for the distortion of the ion distribution function (weak turbulence) but neglects higher order wave-wave

couplings.

Only ions will be used in these calculations. We show in the appendix that for our conditions, the electrons are expected to remain Maxwellian and undergo negligible heating from ion acoustic turbulence.

The code calculates the trajectory of each particle  $[\mathbf{r}(t), \mathbf{v}(t)]$  by integrating its equation of motion:  $m_i d\mathbf{v}/dt = -q_i \sum_k \nabla \phi_k(\mathbf{r}, t)$ , where  $m_i$  is the ion mass and  $q_i = Ze$  is its charge. The integration is carried out with a Runge Kutta method.

If we assume that the laser fields envelopes are constant in time and spatially uniform, then  $\hat{\varphi}_p$  is also constant. It is then straightforward to express the time-evolution of the fields  $\phi_k$  using quasi-linear theory [15–17].

We decompose the ion distribution function into its spatial average and the responses to each of the beat waves' electrostatic potentials:

$$f_i(\mathbf{r}, \mathbf{v}, t) = f_{i0}(\mathbf{v}, t) + \sum_k f_k(\mathbf{r}, \mathbf{v}, t), \quad (24)$$

with  $f_k(\mathbf{r}, \mathbf{v}, t) = \frac{1}{2} \hat{f}_k(t) \exp[i\psi_k] + c.c.$ . Taking the spatial average of the Vlasov equation (Eq. (1)) gives:

$$\frac{\partial f_0}{\partial t} = -\frac{q_i}{2m_i} \sum_k \text{Im} \left[ \mathbf{k} \cdot \frac{\partial \hat{f}_k^*}{\partial \mathbf{v}} \hat{\phi}_k \right], \quad (25)$$

where the linearized plasma perturbation  $\hat{f}_k$  is given by:

$$\hat{f}_k(t) = -\frac{q_i}{m_i} \hat{\phi}_k(t) \mathbf{k} \cdot \frac{\partial f_0(t)}{\partial \mathbf{v}} \frac{1}{\omega_k - \mathbf{k} \cdot \mathbf{v}}. \quad (26)$$

Inserting the latter expression for  $\hat{f}_k$  in Eq. (25) gives the familiar diffusion equation from quasi-linear theory:

$$\frac{\partial f_0(\mathbf{v}, t)}{\partial t} = \frac{\partial}{\partial \mathbf{v}} \cdot \bar{D} \cdot \frac{\partial}{\partial \mathbf{v}} f_0(\mathbf{v}, t) \quad (27)$$

with the quasi-linear diffusion operator:

$$\bar{D} = \frac{q_i^2}{2m_i^2} \sum_k |\hat{\phi}_k|^2 \mathbf{k} \mathbf{k} \text{Im} \frac{1}{\omega_k - \mathbf{k} \cdot \mathbf{v}}. \quad (28)$$

Because the beat waves are externally driven and typically do not verify the ion acoustic resonance condition (i.e. they are *not* ion acoustic waves), the usual assumptions arising at this point in quasi-linear theory, such as the one consisting in separating the frequency into a real component and an infinitesimally small imaginary part [18], is not valid here, and we shall instead pursue the derivation keeping the full expression for the susceptibilities.

Following the same steps as for the linear calculation, we get the following expression for the electrostatic potential  $\phi_k$  associated with the beat wave between the quads  $m$  and  $n$  (with  $\psi_k = \psi_m - \psi_n$ ), which is then used in the equation of motion of the particles:

$$\phi_k(\mathbf{r}, t) = \frac{e}{4r_e} |\hat{a}_m| |\hat{a}_n| \sqrt{1 + \cos^2 \theta_{mn}} \left| \frac{\chi_{ek}}{1 + \chi_{ek} + \chi_{ik}(t)} \right| \times \cos(\mathbf{k} \cdot \mathbf{r} - \omega_k t + \rho_k). \quad (29)$$

The electrons are supposed to remain Maxwellian (cf. appendix), and their thermal velocity ( $v_{Te} = 2.2 \times 10^7$  m/s for  $T_e = 2.8$  keV) is much larger than the phase velocities of the beat waves ( $v_k = [0-4 \times 10^5]$  m/s for  $\Delta\lambda = 6$  Å), so  $\chi_{ek} \simeq 1/(k\lambda_{De})^2$ . The ion susceptibility adiabatically follows the time evolution of the space-averaged distribution function:

$$\chi_{ik}(t) = \sum_j \frac{4\pi q_j^2}{k^2 m_j} \int \mathbf{k} \cdot \frac{\partial f_{ij0}(\mathbf{v}, t)}{\partial \mathbf{v}} \frac{d^3 v}{\omega_k - \mathbf{k} \cdot \mathbf{v}}. \quad (30)$$

The time-averaged distribution function  $f_{ij0}(\mathbf{v}, t)$  for each ion specie  $j$  is calculated for each beat wave by projecting the distribution function along the direction of  $\mathbf{k}$  (for example, let us assume that  $\mathbf{k}$  is along  $x$ ), which reduces the integral to one dimension:

$$\begin{aligned} \chi_{ik}(t) &= \frac{\omega_{pi}^2}{n_i k^2} \int \mathbf{k} \cdot \frac{\partial f_0(t)}{\partial \mathbf{v}} \frac{d^3 v}{\omega_k - \mathbf{k} \cdot \mathbf{v}} \\ &= -\frac{\omega_{pi}^2}{n_i k^2} \int \frac{F_0(v_x)}{\partial v_x} \frac{dv_x}{v_x - v_k}, \end{aligned} \quad (31)$$

where  $F_0(v_x) = \int f_0(\mathbf{v}) dv_y dv_z$ . The integration is performed numerically following the same method as in Ref. [19]. The 1D distribution function  $F_0(v_x)$  is calculated by binning the velocities of all the particles (projected along  $\mathbf{k}$ ). This is the most time-consuming step of the code, since many (276, i.e. one for each beat wave) distributions need to be calculated from a large number of particles (we typically get noise-free results for  $\sim 10^7$  to  $\sim 10^8$  particles). This step is thus split using parallel calculations where each CPU calculates one  $F_0(v_x)$  (which therefore requires 276 CPUs).

Finally, a binary collision scheme is used to calculate collisional effects: at each time step, the particles are shuffled and grouped in pairs (we use the Fisher-Yates algorithm) and each pair  $(\alpha, \beta)$  undergoes an elastic collision, i.e.

$$\begin{aligned} \mathbf{v}_\alpha(t + \delta t) &= \mathbf{v}_\alpha(t) + \frac{\mu_{\alpha\beta}}{m_\alpha} \Delta \mathbf{u}, \\ \mathbf{v}_\beta(t + \delta t) &= \mathbf{v}_\beta(t) - \frac{\mu_{\alpha\beta}}{m_\beta} \Delta \mathbf{u}, \end{aligned} \quad (32)$$

where  $\mu_{\alpha\beta}$  is the reduced mass and  $\Delta \mathbf{u}$  is taken from Takizuka and Abe [20]. This scheme also accounts for collisions between ions of different species.

In summary, our code follows the following steps at each time interval  $t \rightarrow t + \delta t$ :

1. the 3D position and velocity of each particle  $\mathbf{r}(t + \delta t)$ ,  $\mathbf{v}(t + \delta t)$  are calculated by integrating the equation of motion using a Runge-Kutta algorithm;
2. the resulting new particle velocities are projected along the velocity of each beat wave  $\mathbf{k}$  in order to get the 1D distribution  $F_0(v_x)$ ;
3.  $F_0(v_x)$  is then integrated using Eq. (31), following the numerical scheme of Ref. [19], in order to get  $\chi_{ik}(t + \delta t)$  and therefore  $\phi_k(t + \delta t)$  (from Eq. (29));
4. a binary collision scheme is then applied to all the particles, which have subsequently shuffled and grouped in pairs following Ref. [20].

Results from the particle code have recently been presented in Ref. [13] for the case of He; here, we present new results for a multi-species plasma of  $C_5H_{12}$ . Fig. 4 shows the distribution function plotted on a logarithmic scale as a function of  $v_z$  (velocity along the hohlraum axis  $z$ ) and  $v_\perp = \sqrt{v_x^2 + v_y^2}$ , for the hydrogen and carbon ions. Both species are initialized with the same ion temperature  $T_i = 0.8$  keV. The green dots represent the phase velocities of the 276 beat waves previously shown in Fig. 3a.

As shown in Fig. 4, whereas most of the beat waves' phase velocities are of the order of  $v_{Ti}$  or less for the hydrogen ions at  $t=0$  (at most,  $v_k \simeq 2v_{Ti}$  for the fastest beat waves), the phase velocities range from 0 to  $> 10v_{Ti}$  for the carbon ions whose thermal velocity is lower than for the hydrogen ions. Ion heating is observed, similarly to Ref. [13], and after 500 ps, the hydrogen ions have heated to temperatures such that all the beat waves' phase velocities are smaller than  $v_{Ti}$ . On the other hand, the carbon ions keep having beat waves near  $v_{Ti}$  for much longer times, which leads to a stronger and more sustained heating. The carbon distribution function is also noticeably distorted even after 500 ps, as thermalization from ion-ion collisions doesn't quite compensate the distortion from weak turbulence.

Figure 5a shows the temperatures for the two species, showing ion temperatures greater than 10 keV after 1 ns for the carbon ions, whereas the hydrogen ions only heat up to less than 4 keV. Figure 5b shows the CBET gain rates for  $C_5H_{12}$  compared to He (as in Ref. [13]). The gains are overall very similar and decrease at similar rates due to ion heating.

#### IV. SATURATION OF CBET FOR NIF CONDITIONS

##### A. CBET gains for plasma oscillations driven off-resonance

We have shown that stochastic ion heating saturates the CBET mechanism by modifying the local plasma conditions: when the beat waves' phase velocities are close to

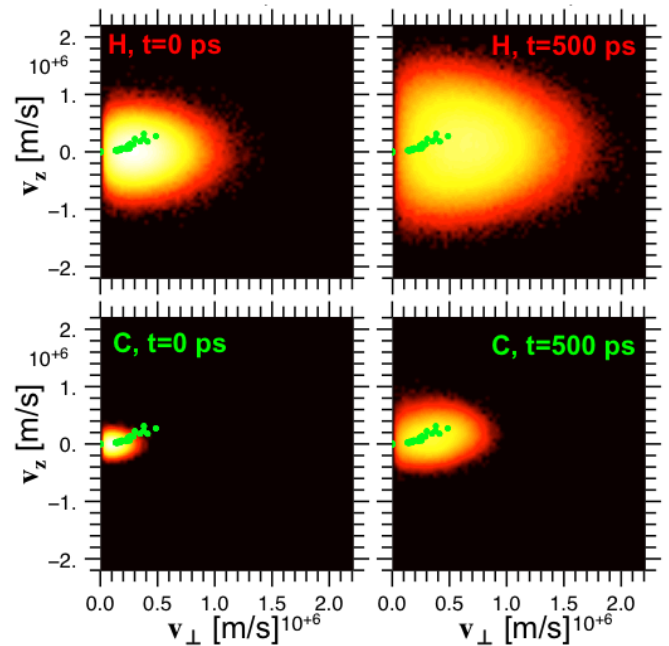


FIG. 4. Distribution function (log scale, arbitrary units) of the hydrogen and carbon ions of a  $C_5H_{12}$  plasma at  $t=0$  (when both species are initially Maxwellian with the same temperature,  $T_i = 0.8$  keV) and after 500 ps, plotted as a function of the longitudinal velocity  $v_z$  (along the hohlraum axis) and the transverse velocity  $v_\perp = \sqrt{v_x^2 + v_y^2}$ . The green dots represent the beat waves' phase velocities (cf. Fig. 3a). Due to the symmetry around the hohlraum axis on NIF (cf. Fig. 2), each green dot marks the position of 4 beat waves symmetrically distributed every  $90^\circ$  in azimuth, and the particle distribution function is essentially axisymmetric around the hohlraum axis.

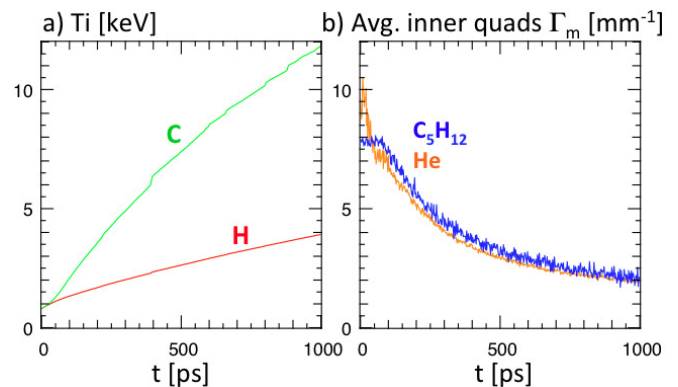


FIG. 5. a) ion temperature (defined in the local Maxwellian limit, i.e.  $\frac{3}{2}k_B T_i = \frac{1}{2}m_i(\langle v^2 \rangle - \langle v \rangle^2)$  for the carbon and hydrogen ions in a  $C_5H_{12}$  plasma with an initial ion temperature  $T_i = 0.8$  keV for the hydrogen and carbon ions; b) average CBET gain rate  $\Gamma_m$  for a NIF inner quad for a  $C_5H_{12}$  plasma and a pure He plasma.

the ion thermal velocity, wave-particle energy exchange and ion-ion collisions heat the bulk of the ion distribution at very fast rates (several keV/ns). The ion temperature tends to stabilize after the ion acoustic velocity has been increased to the point where none of the beat waves are close to resonance anymore. In this limit, most of the beat waves have a phase velocity which is smaller than the thermal velocity of the ions.

We can derive a simplified expression for the CBET gains in this limit of off-resonance driven waves. Similar to Ref. [13], we will assume that the ion-ion collisions thermalize the distribution rapidly enough to justify a local Maxwellian approximation.

The expression for the ion susceptibility given in the linear limit by Eq. (23) can be expressed for the limit of small arguments of the  $Z'$  function when  $v_k = \omega_k/k \ll v_{Ti}$  (we assume that  $\mathbf{V} = 0$  for simplicity; if a finite plasma flow is present  $\omega_k$  should just be replaced by  $\omega_k - \mathbf{k} \cdot \mathbf{V}$ ). This gives:

$$\chi_{ik} \simeq \sum_j \frac{\alpha_j}{\kappa^2} \left[ 1 + i \sqrt{\frac{\pi}{2}} \frac{v_k}{v_{Ti,j}} \right] \quad (33)$$

where  $\kappa = k\lambda_{De}$ ,  $\alpha_j = Z_j^* T_e / T_i$  and  $Z_j^* = f_j Z_j^2 / \bar{Z}$ .

As ions are heated up,  $T_i$  can in principle become of the same order as  $T_e$  so one cannot assume that  $Z T_e / T_i \gg 1$ . Assuming nevertheless that  $1 / (k\lambda_{Di})^2 \gg 1$ , the term  $K_k = \chi_{ek}(1 + \chi_{ik}) / (1 + \chi_{ek} + \chi_{ik})$  in the coupling coefficient can be expressed as:

$$\text{Im}(K_k) \simeq \frac{\text{Im}(\chi_{ik})}{\kappa^4 |\epsilon_k|^2}, \quad (34)$$

where  $\epsilon_k = 1 + \chi_{ek} + \chi_{ik}$ . Using the small phase velocity limit from Eq. (33) for the ion susceptibility gives:

$$|\epsilon_k|^2 \simeq \frac{1}{\kappa^4} \left( 1 + \sum_j \alpha_j \right)^2, \quad (35)$$

and:

$$\text{Im}(\chi_{ik}) \simeq \frac{1}{\kappa^2} \sqrt{\frac{\pi}{2}} \sum_j \alpha_j \frac{v_k}{v_{Ti,j}}. \quad (36)$$

The coupling coefficient thus takes the following form:

$$\text{Im}(K_k) \simeq \sqrt{\frac{\pi}{2}} \frac{v_k}{\kappa^2} \frac{\sum_j \frac{\alpha_j}{v_{Ti,j}}}{\left( 1 + \sum_j \alpha_j \right)^2}. \quad (37)$$

The gain seen by the quad  $m$  (“seed”) from quad  $n$  (“pump”), per Eq. (21), thus takes the following form:

$$\gamma_{mn} = -\sqrt{\frac{\pi}{2}} \frac{\omega_k |\hat{a}_n|^2 (1 + \cos^2 \theta_{mn})}{16k_0^2 \lambda_{De}^2 \sin \theta_{mn} / 2} \frac{\sum_j \frac{\alpha_j}{v_{Ti,j}}}{\left( 1 + \sum_j \alpha_j \right)^2} \quad (38)$$

$$\propto I_n \frac{n_e}{T_e} \Delta\lambda_{mn} \frac{\sum_j \alpha_j / \sqrt{T_{i,j}}}{\left( 1 + \sum_j \alpha_j \right)^2}, \quad (39)$$

where  $\Delta\lambda_{mn}$  is the wavelength difference between the quads  $m$  and  $n$ .

Figure 6 shows the average gain rate for inner quads on NIF vs.  $\Delta\lambda$ , the wavelength shift between inner and outer quads. This curve is calculated using the reduced quasi-linear model described in Ref. [13] (and detailed in the appendix), for a pure He plasma with the same conditions used in the previous sections. The highlighted region shows the typical NIF operational range of  $\Delta\lambda$ , i.e.  $\sim 5$  to  $9 \text{ \AA}$ .

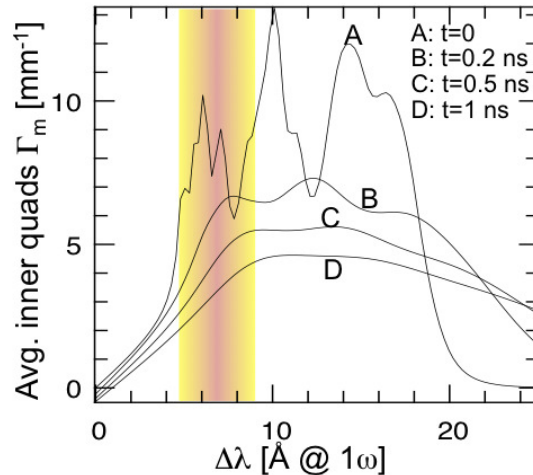


FIG. 6. bla

At  $t=0$ , the curve exhibits significant oscillations between 6 and 14  $\text{\AA}$ . As  $\Delta\lambda$  is increased, some of the beat waves' phase velocities ( $v_k \propto \Delta\lambda$ ) will hit the ion acoustic resonance, i.e.  $v_k = c_s$  where  $c_s$  is the ion acoustic velocity. Each peak in the curve corresponds to a group of beat waves becoming resonant. At later times, ion heating pushes the beat waves off resonance while making these resonance regions broader, thus smoothing the curve out; the gain region extends to longer wavelength separations, beyond 20-25  $\text{\AA}$ .

Because the ion thermal velocity is increased, most of the beat waves get into the regime described above, where  $v_k \ll v_{Ti}$ . As a result, the curve is essentially linear vs.  $\Delta\lambda$  for wavelength shifts up to 8 to 10  $\text{\AA}$ , vs. up to 4  $\text{\AA}$  at  $t=0$ . This is in qualitative agreement with NIF experiments, which indicate linear scalings of power transfer vs.  $\Delta\lambda$  for shifts up to 8  $\text{\AA}$ .

## B. Ion heating and momentum deposition in NIF hohlraums

Finally, we show maps of ion heating rates for NIF hohlraum conditions, using the fluid formulae derived in the appendix. Figure 7a shows the initial ion temperature as calculated by the radiation-hydrodynamics code Lasnex for the upper half of a NIF hohlraum at time of peak laser power. The green contour is the electron

density isocontour at  $n_c/4$ . The ion temperature is calculated to be 4 keV near the LEH in the expanding gold plasma; however the volume where all the laser beams overlap (near  $x=0$  and  $z=5$  mm) is located in a pure helium plasma with  $T_i \simeq 1$  keV.

The heating rate  $dT_i/dt$  is shown in Fig. 7b. Heating rates of 6 to 7 keV/ns are obtained, for a very localized region of  $\sim 1$  mm<sup>3</sup> at the LEH. These rates correspond to an initial increase of  $\sim 60\%$  per 100 ps (we expect the heating to slow down and stabilize after  $\sim 0.5$  ns, as described in Ref [13]).

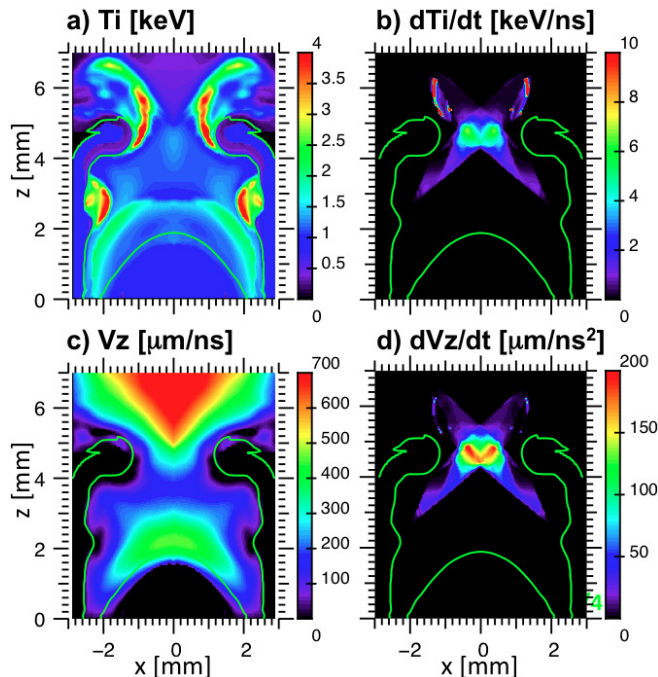


FIG. 7. a) initial ion temperature calculated by the Lasnex code at peak laser power for the upper half of a NIF hohlraum; b) ion heating rate (in keV/ns) calculated by our quasi-linear model; c) initial flow velocity along  $z$  (hohlraum axis) calculated by Lasnex at the same time, and d) acceleration of the flow due to momentum deposition. The green contour represents the  $n_e = n_c/4$  density isocontour.

The wave-particle momentum exchange also leads to an acceleration of the flow at the LEH as shown in Fig. 7d (the initial flow velocity calculated by Lasnex, projected along the  $z$  direction, is shown in Fig. 7c). Because all the beat waves' phase velocities point towards  $z > 0$  (cf. Fig. 3: all the transverse component cancel each other out, but the  $z$  components are all positive and can all add up), the average acceleration is also directed towards  $z > 0$ . The acceleration rate is relatively modest compared to the heating: the flow is being accelerated from its initial value at  $< 5\%$  per 100 ps.

The orientation of the beat waves towards  $z > 0$  is due to the choice of  $\Delta\lambda > 0$ , i.e.  $\lambda_{inners} > \lambda_{outers}$ , because transfer from the outer beams to the inner beams

is currently required on NIF in order to achieve symmetric implosion due to impaired propagation if the inner beams, which undergo stronger than anticipated absorption in the plasma as well as significant backscatter [21].

However, if for any reason  $\Delta\lambda$  had to be set to negative values to transfer power from the inner to the outer beams (as could be the case for a different type of target, for example if the outer beams have more backscatter than the inner beams), then the process would be reversed, and the acceleration from momentum deposition would be directed towards  $z < 0$ , i.e. against the existing flow direction.

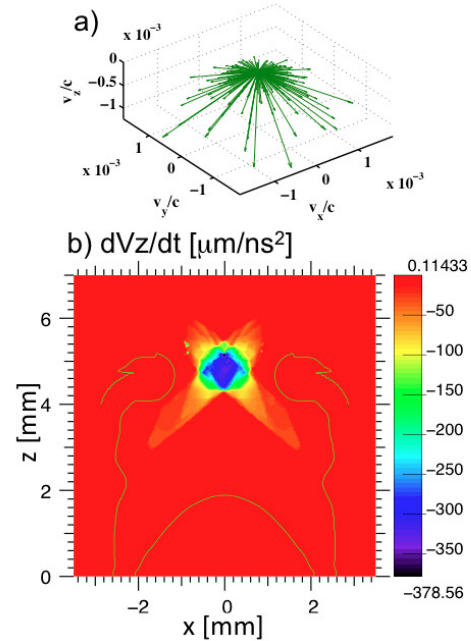


FIG. 8. a) phase velocities of the 276 beat waves for the case where  $\Delta\lambda = \lambda_{inners} - \lambda_{outers} < 0$ , with  $\Delta\lambda = -8$  Å; b) resulting flow acceleration along  $z$ ,  $dV_z/dt$ , showing an expected deceleration of the flow at the LEH ( $dV_z/dt < 0$  whereas the initial flow velocity is positive, as seen in Fig. 7c).

This is what is illustrated in Fig. 8. The beat waves' phase velocities are shown in Fig. 8a for  $\Delta\lambda = -8$  Å. The velocity vectors have their sign reversed compared to Fig. 3. As a result, the flow acceleration along  $z$  is negative, as shown in Fig. 8b. Since the flow is near sonic at the LEH (and supersonic just outside), similarly to a nozzle flow, the drag resulting from momentum deposition in the opposite direction as the flow direction may, under certain conditions, result in the formation of a bow shock [22].

## V. CONCLUSION

In summary, we have shown that stochastic ion heating from many beat waves created by multiple crossing

laser beams can be an efficient saturation mechanism for CBET. For typical wavelength separations on NIF ( $\Delta\lambda \sim 4$  to  $10 \text{ \AA}$ ) and typical ion temperatures (near  $1 \text{ keV}$ ), the phase velocities of the beat waves extend from zero to a few times the thermal velocity, which leads to strong wave-particle coupling. As a result, energy and momentum are both deposited in the plasma. Thermalization from ion-ion collisions transfer the energy gained by energetic particles into the bulk, leading to rapid ion heating. For such conditions, we expect that the ion temperature will rise until the plasma sound speed becomes larger than all the beat waves' phase velocities. At this point, most of the beat waves' phase velocities are also smaller than the ion thermal velocity. In this regime, the laser beams' CBET gains have a linear dependence with  $\Delta\lambda$ , the wavelength shift between cones of laser beams on NIF. Strong heating rates are expected in a  $\sim \text{mm}^3$ -scale volume at the LEH of NIF hohlraums. The plasma flow should also be modified from momentum deposition: in the case of power transfer from "outer" to "inner" beams, as is currently the case for NIF experiments, the flow near the LEH should be accelerated; on the other hand, for experiments where power transfer would be required to occur in the opposite direction, i.e. from the outer beams to the inner beams, the flow would be decelerated near the LEH. A self-consistent hydrodynamics package including a ray-based CBET model, together with the associated ion heating and momentum deposition is currently being tested in the Hydra and Lasnex codes.

### Appendix: Reduced fluid model and estimates of electron heating

The quasi-linear theory can be used to calculate the evolution of the momentum and temperature. If the collisions thermalize the ion distribution rapidly enough, then a local Maxwellian approximation can be used.

The momentum evolution is given by:

$$\frac{d\mathbf{V}}{dt} = \frac{1}{n_i} \int d^3v \frac{\partial f_0(\mathbf{v}, t)}{\partial t} \mathbf{v}. \quad (\text{A.1})$$

Replacing  $\partial_t f_0$  by its expression from Eq. (25) and integrating by parts gives:

$$\frac{d\mathbf{V}}{dt} = \frac{-1}{8\pi n_i m_i} \sum_k |\hat{\phi}_k(t)|^2 k^2 \mathbf{k} \text{Im}(\chi_{ik}(t)). \quad (\text{A.2})$$

The energy gained (or lost) by the fluid as kinetic energy is  $dU_{flow}/dt = m_i \mathbf{V} d\mathbf{V}/dt$ , i.e.:

$$\frac{dU_{flow}}{dt} = \frac{-1}{8\pi n_i} \sum_k |\hat{\phi}_k(t)|^2 k^2 \mathbf{k} \cdot \mathbf{V} \text{Im}(\chi_{ik}(t)). \quad (\text{A.3})$$

Similarly, the total energy (kinetic + thermal) gained by the ion fluid is  $dU_{tot}/dt = \frac{1}{2} m_i \langle v^2 \rangle$ , i.e.:

$$\frac{dU_{tot}}{dt} = \frac{m_i}{2n_i} \int d^3v \mathbf{v}^2 \frac{\partial f_0(\mathbf{v}, t)}{\partial t}. \quad (\text{A.4})$$

The integration gives:

$$\frac{dU_{tot}}{dt} = \frac{1}{8\pi n_i} \sum_k |\hat{\phi}_k(t)|^2 k^2 \omega_k \text{Im}(\chi_{ik}(t)). \quad (\text{A.5})$$

This is the usual wave-particle energy conservation relation from quasi-linear theory, i.e.:

$$\frac{d}{dt} \left( n_i \int_{-\infty}^{\infty} \frac{m_i v^2}{2} f_0(\mathbf{v}, t) d^3v \right) = \sum_k \gamma_k \frac{|\hat{E}_k|^2}{8\pi}, \quad (\text{A.6})$$

where  $\hat{E}_k = -ik\hat{\phi}_k$ , and  $\gamma_k = -\omega_k \text{Im}(\chi_{ik})$  is the wave's growth rate.

The temperature can simply be derived as  $\frac{3}{2} k_B T_i = \frac{1}{2} m_i [\langle v^2 \rangle - \langle v \rangle^2] = U_{tot} - U_{flow}$ , which gives:

$$\frac{dk_B T_i}{dt} = \frac{1}{12\pi n_i} \sum_k |\hat{\phi}_k(t)|^2 k^2 (\omega_k - \mathbf{k} \cdot \mathbf{V}) \text{Im}(\chi_{ik}(t)). \quad (\text{A.7})$$

The two equations for the momentum and temperature, Eqs. (A.7) and (A.2), can be coupled via the quasi-linear expression of  $\chi_{ik}(t)$  assuming a local Maxwellian, which reads:

$$\chi_{ik}(t) = \frac{-1}{2(k\lambda_{Di})^2} Z' \left[ \frac{\omega_k - \mathbf{k} \cdot \mathbf{V}(t)}{\sqrt{2} k v_{Ti}(t)} \right]. \quad (\text{A.8})$$

Finally, we can also estimate the effect of the beat waves on the electron temperature. The derivation is similar to the one for the ions, except for the force in the Vlasov equation which must account for the ponderomotive potential in addition to the electrostatic potential for each beat wave, with  $\hat{\varphi}_{p,k} + \hat{\phi}_k = -(1 + \chi_{ik}) \hat{\phi}_k / \chi_{ek}$ . To estimate the effect of weak turbulence on the electrons compared to the ions, we express the total energy gained by the electron fluid:

$$\frac{dU_{e,tot}}{dt} = \frac{1}{8\pi n_e} \sum_k |\hat{\phi}_k(t)|^2 \left| \frac{1 + \chi_{ik}}{\chi_{ek}} \right|^2 k^2 \omega_k \text{Im}(\chi_{ek}(t)). \quad (\text{A.9})$$

This means that for an infinitesimal time step, the energy increment due to each beat wave for the electrons,  $\delta U_{ek}$ , and the ions,  $\delta U_{ik}$ , have the following ratio:

$$\frac{\delta U_{ek}}{\delta U_{ik}} = \frac{1}{Z} \frac{\text{Im}(\chi_{ek})}{\text{Im}(\chi_{ik})} \left| \frac{\chi_{ek}}{1 + \chi_{ik}} \right|^2. \quad (\text{A.10})$$

If the driven wave is an ion acoustic wave, in which case its wavelength and frequency exactly verify  $v_k = c_s$ , then  $\epsilon_k = 1 + \chi_{ek} + \chi_{ik} = 0$  and the last term on the right-hand side equals 1. The ratio of electron vs. ion heating is then simply equal to the ratio of electron vs. ion Landau damping, which is expected to be negligible for ion acoustic waves. This will typically not be the case for NIF since the phase velocities are externally prescribed and typically verify  $v_k \ll c_s$ , but the electron heating will still be negligible, in fact even more so than for a pure ion acoustic wave.

To make this more evident, we take the limit of small  $\Delta\lambda$ , where  $v_k \ll v_{T_i}$  (and *a fortiori*,  $v_k \ll v_{T_e}$ ). In this limit, we have:

$$\chi_{ek} \simeq \frac{1}{\kappa^2} \left[ 1 + i \sqrt{\frac{\pi}{2}} \frac{v_k}{v_{T_e}} \right], \quad (\text{A.11})$$

$$\chi_{ik} \simeq \frac{ZT_e}{T_i} \frac{1}{\kappa^2} \left[ 1 + i \sqrt{\frac{\pi}{2}} \frac{v_k}{v_{T_i}} \right], \quad (\text{A.12})$$

where  $\kappa = k\lambda_{De}$ . Therefore we get:

$$\frac{\delta U_{ek}}{\delta U_{ik}} \simeq \sqrt{\frac{m_e}{Zm_i}} \left( \frac{T_i}{ZT_e} \right)^{3/2} \frac{1}{((ZT_e/T_i) + \kappa^2)} \quad (\text{A.13})$$

or:

$$\frac{\delta U_{ek}}{\delta U_{ik}} \simeq \sqrt{\frac{m_e}{Zm_i}} \left( \frac{T_i}{ZT_e} \right)^{7/2} \quad (\text{A.14})$$

if  $ZT_e/T_i \ll \kappa^2$ .

It is now evident that the energy going into the electrons is negligible compared to that going into the ions. For example, for a helium plasma with  $T_e = T_i$ , we have  $\delta U_{ek} \simeq 1.5 \times 10^{-3} \delta U_{ik}$ .

## ACKNOWLEDGMENTS

We gratefully acknowledge useful discussions with Harvey Rose and Wally Manheimer. This work was performed under the auspices of the U.S. Department of Energy by Lawrence Livermore National Laboratory under Contract DE-AC52-07NA27344.

- 
- [1] W. L. Kruer, S. C. Wilks, B. B. Afeyan, and R. K. Kirkwood, *Phys. Plasmas* **3**, 382 (1996).
- [2] V. V. Eliseev, W. Rozmus, V. T. Tikhonchuk, and C. E. Capjack, *Phys. Plasmas* **6**, 3 (1996).
- [3] P. Michel, L. Divol, E. A. Williams, S. Weber, C. A. Thomas, D. A. Callahan, S. W. Haan, J. D. Salmonson, S. Dixit, D. E. Hinkel, M. J. Edwards, B. J. MacGowan, J. D. Lindl, S. H. Glenzer, and L. J. Suter, *Phys. Rev. Lett.* **102**, 025004 (2009).
- [4] S. H. Glenzer, B. J. MacGowan, P. Michel, N. B. Meezan, L. J. Suter, S. N. Dixit, J. L. Kline, G. A. Kyrala, D. K. Bradley, D. A. Callahan, E. L. Dewald, L. Divol, E. Dzenitis, M. J. Edwards, A. V. Hamza, C. A. Haynam, D. E. Hinkel, D. H. Kalantar, J. D. Kilkenny, O. L. Landen, J. D. Lindl, S. LePape, J. D. Moody, A. Nikroo, T. Parham, M. B. Schneider, R. P. J. Town, P. Wegner, K. Widmann, P. Whitman, B. K. F. Young, B. Van Wouterghem, L. J. Atherton, and E. I. Moses, *Science* **327**, 1228 (2010).
- [5] P. Michel, S. H. Glenzer, L. Divol, D. K. Bradley, D. Callahan, S. Dixit, S. Glenn, D. Hinkel, R. K. Kirkwood, J. L. Kline, W. L. Kruer, G. A. Kyrala, S. L. Pape, N. B. Meezan, R. Town, K. Widmann, E. A. Williams, B. J. MacGowan, J. Lindl, and L. J. Suter, *Phys. Plasmas* **17**, 056305 (2010).
- [6] P. Michel, L. Divol, R. P. J. Town, M. D. Rosen, D. A. Callahan, N. B. Meezan, M. B. Schneider, G. A. Kyrala, J. D. Moody, E. L. Dewald, K. Widmann, E. Bond, J. L. Kline, C. A. Thomas, S. Dixit, E. A. Williams, D. E. Hinkel, R. L. Berger, O. L. Landen, M. J. Edwards, B. J. MacGowan, J. D. Lindl, C. Haynam, L. J. Suter, S. H. Glenzer, and E. Moses, *Phys. Rev. E* **83**, 046409 (2011).
- [7] J. D. Moody, P. Michel, L. Divol, R. L. Berger, E. Bond, D. K. Bradley, D. A. Callahan, E. L. Dewald, S. Dixit, M. J. Edwards, S. Glenn, A. Hamza, C. Haynam, D. E. Hinkel, N. Izumi, O. Jones, J. D. Kilkenny, R. K. Kirkwood, J. L. Kline, W. L. Kruer, G. A. Kyrala, O. L. Landen, S. LePape, J. D. Lindl, B. J. MacGowan, N. B. Meezan, A. Nikroo, M. D. Rosen, M. B. Schneider, D. J. Strozzi, L. J. Suter, C. A. Thomas, R. P. J. Town, K. Widmann, E. A. Williams, L. J. Atherton, S. H. Glenzer, and E. I. Moses, *Nature Phys.* **8**, 344 (2012).
- [8] I. V. Igumenshchev, W. Seka, D. H. Edgell, D. T. Michel, D. H. Froula, V. N. Goncharov, R. S. Craxton, L. Divol, R. Epstein, R. Follett, J. H. Kelly, T. Z. Kosc, A. V. Maximov, R. L. McCrory, D. D. Meyerhofer, P. Michel, J. F. Myatt, T. C. Sangster, A. Shvydky, S. Skupsky, and C. Stoeckl, *Physics of Plasmas* **19**, 056314 (2012).
- [9] D. H. Froula, I. V. Igumenshchev, D. T. Michel, D. H. Edgell, R. Follett, V. Y. Glebov, V. N. Goncharov, J. Kwiatkowski, F. J. Marshall, P. B. Radha, W. Seka, C. Sorce, S. Stagnitto, C. Stoeckl, and T. C. Sangster, *Phys. Rev. Lett.* **108**, 125003 (2012).
- [10] E. A. Williams, D. E. Hinkel, and J. A. Hittinger, in *Inertial Fusion Sciences and Applications 2003* (The American Nuclear Society, 2004) p. 252.
- [11] E. A. Williams, B. I. Cohen, L. Divol, M. R. Dorr, J. A. Hittinger, D. E. Hinkel, A. B. Langdon, R. K. Kirkwood, D. H. Froula, and S. H. Glenzer, *Phys. Plasmas* **11**, 231 (2004).
- [12] R. P. J. Town, M. D. Rosen, P. A. Michel, L. Divol, J. D. Moody, G. A. Kyrala, M. B. Schneider, J. L. Kline, C. A. Thomas, J. L. Milovich, D. A. Callahan, N. B. Meezan, D. E. Hinkel, E. A. Williams, R. L. Berger, M. J. Edwards, L. J. Suter, S. W. Haan, J. D. Lindl, E. L. Dewald, S. Dixit, S. H. Glenzer, O. L. Landen, E. I. Moses, H. A. Scott, J. A. Harte, and G. B. Zimmerman, *Physics of Plasmas* **18**, 056302 (2011).
- [13] P. Michel, W. Rozmus, E. A. Williams, L. Divol, R. L. Berger, R. P. J. Town, S. H. Glenzer, and D. A. Callahan, *Phys. Rev. Lett.* **109**, 195004 (2012).
- [14] D. A. Callahan, N. B. Meezan, S. H. Glenzer, A. J. MacKinnon, L. R. Benedetti, D. K. Bradley, J. R. Celeste, P. M. Celliers, S. N. Dixit, T. Döppner, E. G. Dzenitis, S. Glenn, S. W. Haan, C. A. Haynam, D. G. Hicks, D. E. Hinkel, O. S. Jones, O. L. Landen, R. A. London, A. G. MacPhee, P. A. Michel, J. D. Moody, J. E. Ralph, H. F. Robey, M. D. Rosen, M. B. Schneider, D. J. Strozzi, L. J. Suter, R. P. J. Town, K. Widmann, E. A. Williams, M. J. Edwards, B. J. MacGowan, J. D. Lindl, L. J. Atherton,

- ton, G. A. Kyrala, J. L. Kline, R. E. Olson, D. Edgell, S. P. Regan, A. Nikroo, H. Wilkins, J. D. Kilkenny, and A. S. Moore, *Physics of Plasmas* **19**, 056305 (2012).
- [15] W. E. Drummond and D. Pines, *Nucl. Fusion Suppl.* **3**, 1049 (1962).
- [16] A. A. Vedenov, E. P. Velikhov, and R. Z. Sagdeev, *Nucl. Fusion* **1**, 82 (1961).
- [17] I. B. Bernstein and F. Engelmann, *Physics of Fluids* **9**, 937 (1966).
- [18] R. J. Goldston and P. H. Rutherford, *Introduction to plasma physics* (McGraw-Hill Publishing Company, 1968).
- [19] J. P. Palastro, J. S. Ross, B. Pollock, L. Divol, D. H. Froula, and S. H. Glenzer, *Phys. Rev. E* **81**, 036411 (2010).
- [20] T. Takizuka and H. Abe, *Journal of Computational Physics* **25**, 205 (1977).
- [21] M. Rosen, H. Scott, D. Hinkel, E. Williams, D. Callahan, R. Town, L. Divol, P. Michel, W. Kruer, L. Suter, R. London, J. Harte, and G. Zimmerman, *High Energy Density Physics* **7**, 180 (2011).
- [22] H. A. Rose *et al.*, (in preparation).